Journal of Molecular Structure 1239 (2021) 130484

Contents lists available at ScienceDirect

Journal of Molecular Structure

journal homepage: www.elsevier.com/locate/molstr

Novel antioxidant quinoxaline derivative: Synthesis, crystal structure, theoretical studies, antidiabetic activity and molecular docking study

Mohcine Missioui[a], Salma Mortada[b], Walid Guerrab[a], Goncagül Serdaroğlu[c], Savaş Kaya[d], Joel T. Mague[e], El Mokhtar Essassi[f], My El Abbes Faouzi[b], Youssef Ramli[a,*]

[a] Laboratory of Medicinal Chemistry, Drug Sciences Research Center, Faculty of Medicine and Pharmacy, Mohammed V University in Rabat, Rabat Morocco
[b] Laboratories of Pharmacology and Toxicology, Faculty of Medicine and Pharmacy, Mohammed V University in Rabat, Rabat, Morocco
[c] Sivas Cumhuriyet University, Math. and Sci. Edu., 58140, Sivas, Turkey
[d] Sivas Cumhuriyet University, Health Services Vocational School, Department of Pharmacy, 58140, Sivas, Turkey
[e] Department of Chemistry, Tulane University, New Orleans, LA 70118, United States
[f] Laboratoire de Chimie Organique Hétéerocyclique, Faculté des Sciences, Université Mohammed V in Rabat, Rabat Morocco

ARTICLE INFO

Article history:
Received 24 February 2021
Revised 15 April 2021
Accepted 16 April 2021
Available online 21 April 2021

Keywords:
Quinoxaline
Crystal
Theoretical studies
Antioxidant
Antidiabetic
Docking

ABSTRACT

New quinoxaline derivative, *N*-(4-methyl-2-nitrophenyl)-2-(3-methyl-2-oxoquinoxalin-1(2H)-yl)acetamide (NPOQA) has been synthesized and characterized by IR, ^{1}H &^{13}C NMR, ESI-MS and single crystal X-ray diffraction analysis using experimental and theoretical methods. The thermodynamic quantities and quantum chemical parameters were predicted by using B3LYP/6–311G** level to investigate the physical and electronic properties of the compound. Frontier Molecular Orbital "**FMO**" and Natural Bond Orbital "**NBO**" analyses of the compound were performed to enligten the possible rectivity trend and intramolecular interactions contibuted to the decreasing of the stabilization. In addition, the newly synthesized compound was evaluated for its *in vitro* antidiabetic activity against α-glucosidase and α-amylase enzymes and for antioxidant activity by utilizing several tests as DPPH (1, 1-diphenyl-2-picryl hydrazyl), ABTS (2, 2′-azino-bis(3-ethyl benzthiazoline-6-sulfonicacid), reducing power test (FRAP) and Hydrogen Peroxide Activity H_2O_2. Finally, Molecular docking studies were performed to investigate the binding mode between the quinoxaline derivative NPOQA and α-glucosidase and α-amylase. Docking calculations showed an important binding affinity as compared to standard drug acarbose, -6.5 and -6.9 kcal/mol successively for α-glucosidase and α-amylase, which are in agreement with the results of *in vitro* studies.

1. Introduction

The study of nitrogen heterocycles compounds consists in one of the main branches of organic chemistry due to their role in all kinds of biological processes [1]. The presence of nitrogen-based heterocyclic nuclei has proven to be key for developing thermotropic liquid crystals, notably as a rigid core, and important scaffold for this application is quinoxaline [2–5]. Thus, quinoxaline and its derivatives have been extensively studied play an interesting role as basic skeleton for the synthesis of many other pharmacologically and biologically active agents [6,7]. Notably, these *N*-heterocycles have been reported to exhibit antidiabetic [7] and antioxidant activities [8,9]. Similarly, a wide variety of molecules including *N*-aryl acetamides have been reported in last few years to act as potential antidiabetic agent [10–12] and as antioxidant agent [13,14]. In 2019, according to the International Diabetes Federation (IDF) an estimated 4.2 million deaths were assigned to high blood-glucose levels; It affects 463 million people worldwide and this number is projected to rise to 700 million by 2045, around 25% of the World's population in both developed and developing countries [15]. Therefore, the therapeutic use of antioxidants in the treatment and prevention of diabetic complications has been considered [16]. Many studies have searched for effective and safe inhibitors of α-amylase and α-glucosidase [17–22], from medicinal plants or from chemical synthetic products [23–26], to treat Type 2 diabetes mellitus (T2DM). The purpose of the current work is to synthesize novel quinoxaline-*N*-aryl acetamide hybrid system and evaluate it as antidiabetic and antioxidant agent, so, in continuation of our recent work focused on the synthesis and biological evaluation of novel heterocyclic compounds [27–31], herein, our results are presented.

* Corresponding author.
E-mail address: y.ramli@um5s.net.ma (Y. Ramli).

https://doi.org/10.1016/j.molstruc.2021.130484
0022-2860/

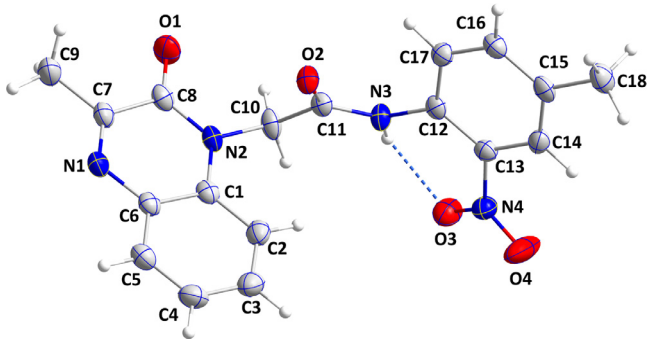

Fig. 1. ORTEP view of the molecular structure of NPOQA with labeling scheme and 50% probability ellipsoids. The intramolecular hydrogen bond is depicted by a dashed line.

2. Experimental section

2.1. Synthesis and crystallization of N-(4-methyl-2-nitrophenyl)−2-(3-methyl-2-oxoquinoxalin-1(2H)-yl)acetamide (NPOQA)

All commercial chemicals were purchased from Sigma-Aldrich and used as received. Follow up of the reaction and checking the purity of the compound were made by TLC on silica gel-precoated aluminum sheets (Fluorescent indicator 254 nm, Fluka, Germany) and the spots were detected by exposure to UV lamp at λ 254/366 nm for few seconds. The melting point was obtained on a Büchi Melting Point SMP-20 apparatus and is uncorrected. The ^{1}H NMR and ^{13}C NMR spectra were recorded on a Bruker Avance 300 NMR Spectrometer in DMSO–*d*6. The chemical shifts δ are reported in parts per million (ppm); the IR spectrum was obtained using the Bruker-VERTEX 70 device and the associated software OPUS, in ATR (attenuated total reflectance) mode. Mass spectra were recorded on an API 3200 LC/MS/MS mass spectrometer using electrospray ionization (ESI) in positive polarity.

(2 g, 12.4 mmol) of 3-methylquinoxalin-2(1H)-one, was dissolved in dimethylformamid (DMF) then added (3.4 g, 14,8 mmol) of 2–chloro-N-(4-methyl-2-nitrophenyl)acetamide, for the removal of the proton we used potassium bicarbonate as a base (2.5 g, 18.6 mmol), for the phase transfer catalysis conditions a tip of a spatula of the BTBA was used, then stirred for 2 h under reflux at 80 °C. After the consumption of the starting reagents, a 500 ml of water was added to the reaction mixture, the main product precipitated, then filtered and dried and recrystallized from ethanol.

2.2. Single crystal X-ray structure determination

A single Pale red crystal with dimension 0.31 × 0.22 × 0.07 mm^3 of the compound was selected and X-ray intensity data were collected at 150 K on a Bruker Smart APEX CCD diffractometer equipped with an X-ray generator operating at 50 kV and 40 mA, using Mo-Kα radiation of wave length 0.71073 Å. The complete sphere of data was processed using SAINT [32]. The structure (Fig. 1) was solved by direct methods and refined by full-matrix least squares method on F2 using SHELXT and SHELXL programs [33,34]. The molecular and packing diagrams were generated using DIAMOND [35]. Crystal and refinement details are presented in Table 1.

CCDC 2,053,356 contains the supplementary crystallographic data for this paper. These data can be obtained free of charge via http://www.ccdc.cam.ac.uk/conts/retrieving.html (or from the Cambridge Crystallographic Data centre, 12, Union Road, Cambridge CB2 1EZ, UK; fax: +44 1223 336,033).

Table 1
Crystal data and structure refinement details.

Value	Parameter
Chemical formula	$C_{18}H_{16}N_4O_4$
M_r	352.35
Crystal system	Triclinic
Space group	P -1
Temperature (K)	150
θ min, θ max	4.4, 72.5°
a, *b*, *c* (Å)	4.560 (2), 13.286 (7), 14.199 (7)
α, β, γ (°)	104.895 (6), 93.352 (7), 91.677 (7)
V (Å^3)	829.0 (8)
Z	2
Radiation type	Mo *Ka*
μ (mm^{-1})	0.10
Crystal size (mm)	0.31 × 0.22 × 0.07
Diffractometer	Bruker Smart *APEX* CCD
Absorption correction	Multi-scan *TWINABS* (Sheldrick, 2009) [36]
T_{min}, T_{max}	0.97, 0.99
No. of measured, independent and observed [$I > 2\sigma(I)$] reflections	12,368, 12,368, 9222
R_{int}	0.023
(sin $\theta/\lambda)_{max}$ (Å^{-1})	0.690
R [$F^2 > 2\sigma(F^2)$], w$R(F^2)$, S	0.045, 0.129, 1.10
No. of reflections	12,368
No. of parameters	286
H-atom treatment	H-atom parameters constrained
$\Delta\rho_{max}$, $\Delta\rho_{min}$ (e Å^{-3})	0.29, −0.28

2.3. Computational and theoretical study

All DFT/B3LYP level [37,38] computations of the compound NPOQA were performed at 6–311G** basis set [39,40], in both the gas and water media. In water environment simulation, PCM "Polarized Continuum Model" [41-43] was used. The frequency calculations were performed for both the structure verification of the compound and to get the thermochemical and physicochemical quantities. After affirming of the structure, the possible reactivity tendency was calculated by using the FMO "Frontier Molecular Orbital" energies. In this context, Koopmans' Theorem [44] has defined the "the ionization energy (I) and electron affinity (A)" via using the HOMO and LUMO energies as follows

$$I = -E_{HOMO}$$
$$A = -E_{LUMO}$$

Then, the (I) and (A) values have been used for calculating the global reactivity identifiers, referring on the CDFT (Conceptual Density Functional Theory) [45–48] as follows.

$$\chi = -\frac{I+A}{2}$$

$$\eta = \frac{I-A}{2}$$

$$\omega = \frac{\mu^2}{2\eta}$$

$$\Delta N_{max} = \frac{I+A}{2(I-A)}$$

Here, these values define as follows χ "electronic chemical potential", η "global hardness", ω "electrophilicty", and ΔNmax "maximum charge transfer capability".

In addition, two useful parameters hae been introduced as ω^- "the electrodonating power" and ω^+ "the electroaccepting power" terms [49], and they have been calculated by the following formulae.

$$\omega^+ \approx (I+3A)^2/(16(I-A))$$

$$\omega^{-} \approx (3I + A)^2/(16(I - A))$$

Furthermore, the back donation contribution to the chemical behavior is also important in the molecular systems, and Gomez and coworkers [50] have introduced $\Delta E_{back\text{-}donation}$ "back-donation energy" as follows.

$$\Delta\varepsilon_{back-donation} = -\frac{\eta}{4}$$

The NBO "Natural Bond Orbital" study introduced by Weinhold et al. [51–54] was performed to estimate the intramolecular interactions. Based on the NBO, the lowering of the stabilization energy has been defined as below, with q_i "bonding orbital occupancy", εi and εj "bonding and antibonding orbital energies" (diagonal elements) and the off-diagonal NBO Fock matrix element.

$$E^{(2)} = \Delta E_{ij} = qi\frac{(Fij)^2}{(\varepsilon j - \varepsilon i)}$$

G09W [55] and GausView 6.0.16 [56] packages were used to perform all quantum chemical computations and pictorial representations of the related results, respectively.

2.4. Antidiabetic study

ρ-Nitrophenyl-α-D-glucopyranoside (pNPG), α-glucosidase from Saccharomyces cerevisiae, α-amylase from Bacillus licheniformis, buffer Solution, DMSO (Dimethylsulfoxide): organic polar solvent for solubilizing products, Sodium Carbonate: solution to stop the reaction, acarbose. All other reagents and standards were of analytical reagent (AR) grade.

In this investigation the synthesized compound was evaluated for the antidiabetic action via two *in-vitro* assays namely, α-amylase and α-glucosidase inhibition method and results were compared with acarbose standard reference in both α-glucosidase and α-amylase methods.

2.4.1. α-glucosidase inhibition assay

The α-glucosidase inhibitory activity of the compound NPOQA was performed by using ρ-nitrophenyl-α-D-glucopyranoside (ρNPG)) as a substrate according to the method described by Kee et al. [57] With minor modifications. The α-glucosidase method is based on the inhibition of the enzyme.α-glucosidase, which hydrolyses pNPG (4-Nitrophenyl-α-D-glucopyranoside) to α-D-glucopyranose and P-nitrophenol of yellow color. The target compound was dissolved in DMSO and all the evaluated samples were dissolved in tampon phosphqate at a series of different concentrations such as 500, 250, 125, 62, 5 and 31,25 µM. The desired concentrations of enzyme were prepared in PBS (pH 6.8, 50 mM). A mixture of 150 µl of the sample and 100 µl of PBS (pH = 6.7) containing the α-glucosidase enzyme solution (0.1 U / ml) was incubated at 37 °C for 10 min, after incubation, 200 µl of pNPG (1 mM) was added to the mixture . The mixtures were incubated at 37 °C for 30 min. Then 1 ml Na_2CO_3 (0.1 M) was added to stop the reaction and the absorbance (Abs) was measured at 405 nm. The result of the antidiabetic activity of our synthesis product was expressed in percentage of inhibition of enzymes studied according to the following formula:

$$Inhibition(\%) = \left(\frac{Abs\ \mathbf{Control} - AbsCompound}{AbsControl}\right) * 100$$

Where $\mathbf{Abs_{Control}}$ refers to the absorbance of control (enzyme and buffer), $\mathbf{Abs_{Compound}}$ refers to the absorbance of sample (enzyme and inhibitor).

Acarbose was used as a positive control to compare the obtained results. The same reaction mixture without α-glucosidase was used as negative control where no improvement in absorbance was observed.

2.4.2. α-amylase inhibition assay

The α-amylase assay was performed by reacting various concentrations of the compound *NPOQA* with α-amylase and starch solution by following the DNSA method with minor modification [58]. The target compounds were dissolved in DMSO and all the evaluated samples were dissolved in tampon phosphqate with various concentrations.

The sample solution (10μL) was mixed with 240μL (sodium phosphate buffer 0.02 M pH6.9) containing α-amylase (240 U/mL), and incubated at 37 °C for 20 min. After pre-incubation, 250 µL of 1% starch solution (1%, sodium phosphate buffer 0.02, pH 6.9) were added to each tube and incubated for 15 min. Add 1 ml of dinitrosalicylic acid to stop the reaction, then incubate the solution in a water bath at 90 °C for 10 min. The mixture was diluted with 1 mL deionized water and the absorbance (Abs) was measured at 540 nm.

The percentage inhibitions were tested at different concentrations, and the IC_{50} values were determined. The control sample was prepared without α-amylase and acarbose was used as a standard drug (positive control).

2.5. Docking methodology

The molecular docking study was performed to investigate the binding mode between the compound NPOQA and α-glucosidase and α-amylase. The preparation of the proteins/ligands, generation of receptor grid, and docking were performed on AutoDock 1.5.6 as described [59]. The 3D structure of the compound *N*-(4-methyl-2-nitrophenyl)−2-(3-methyl-2-oxoquinoxalin-1(2H)-yl)acetamide was obtained using CIF file after crystallization and DRX study. The 3D structure of acarbose was prepared and optimized using molecular builder module implemented in ChemDraw. Gasteiger partial charges were added, nonpolar hydrogen atoms were merged and rotatable bonds were defined. The crystal structure of α-amylase (PDB Id: 4GQR; resolution 1.2 Å) [60] and α-glucosidase (PDB Id: 5NN5; resolution 2.0 Å) [61] were downloaded from the PDB database (http://www.rcsb.org/pdb). AutoDock tool (ADT) was employed to prepare proteins by adding missing hydrogen atoms, assigning Kollman united atom type charges. Grid maps of 40 - 48 −70 Å and 72- 60 −70 Å dimensions with 0.375 Å spacing were prepared using AutoGrid. Other AutoDock parameters were set at their default values. Molecular docking employed the Lamarck Genetic Algorithm (LGA) and the Solis and Wets search methods. And for comparison, molecular docking of reference inhibitor (acarbose) was carried out with α-amylase and α-glucosidase.

2.6. Antioxidant activity

DPPH (2,2-diphenyl-1-picrylhydrazyl), ABTS (2,2′-Azinobis-(3-Ethylbenzthiazolin-6-Sulfonic Acid), (H_2O_2) hydrogen peroxide and ascorbic acid were purchased from Sigma–Aldrich. All other reagents and standards were of analytical reagent (AR) grade.

2.6.1. Radical scavenging activity dpph

The DPPH radical activity assay was performed following [62] with minor modification. The method using the stable free radical 2,2-diphenyl-1-picrylhydrazyl (DPPH) is based upon the reduction of DPPH free radical. Different concentrations of the prepared compound (500, 250, 125, 62.5, 31.25 µM) were tested. The DPPH solution was prepared by dissolving 3,9 mg of DPPH in 50 mL of the methanol. Then, 50µL of each concentration was added to 1,2 ml of methanol and 250µL of the prepared DPPH solution (0.02 mM). The reaction mixture incubated in the dark for 30 min. The control was prepared by adding 1,25 mL of methanol to 250 µL of DPPH. Ascorbic acid was used as the standard. The

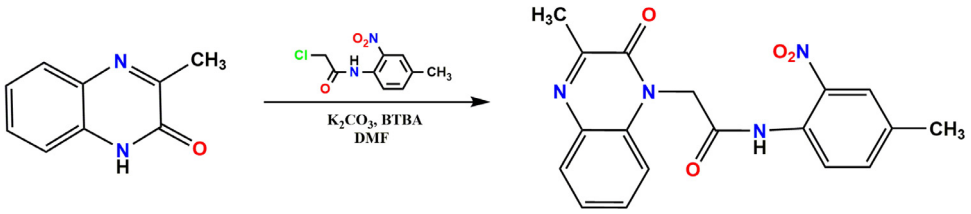

Scheme 1. Synthesis procedure for preparation of (NPOQA).

absorbances of solutions were spectrophotometrically examined at 517 nm. The radical activity is expressed as inhibition ratio of initial concentration of DPPH radical and is calculated according to the formula:

$$\mathbf{DPPH(\%) = [(Abs_{DPPH} - Abs_{Sample})/Abs_{DPPH}] * 100}$$

Where Abs_{DPPH} is the absorbance of DPPH radical and Abs_{sample} is the absorbance in the presence of sample. The activity result in this assay was expressed as IC_{50}, which represents the concentration of the sample required to inhibit 50% of the free radical activity.

2.6.2. Radical scavenging activity abts

The ABTS assay was performed as previously described by Tuberoso et al. [63] ABTS+ radical were generated by oxidation of ABTS with potassium persulfate. The blue-green ABTS was produced through the reaction between 2 mM ABTS and 70 mM potassium persulfate in water. The mixture was left to stand in the dark for 12–16 h before use. The ABTS+ solution as diluted with methanol to an absorbance of 0.700 ± 0.005 at 734 nm. Then 2 mL of diluted ABTS solution were mixed with 100 μL of samples and absorbance was measured after 1 min incubation at room temperature. A standard curve was obtained by using Ascorbic acid as standard solution. The results were expressed as μM Ascorbic acid equivalent.

2.6.3. Ferric reducing power assay (FRAP)

The ferric ion (Fe3+) reducing power assay was performed as previously described by Amarowicz et al. [64] with minor modifications. Briefly, 1 mL of the samples were mixed with 2.5 mL of 0.2 M sodium phosphate buffer (pH 6.6) and 2.5 mL of 1% potassium ferricyanide. The mixtures were incubated in a boiling water bath at 50 °C for 2 min. Then, 2.5 mL of 10% trichloroacetic acid was added and centrifuged at 3000 rpm for 10 min. Finally, 2.5 mL of the supernatant were mixed with 2.5 mL distilled water and 0.5 mL $FeCl_3$ solution (0.1%, w/v). The absorbance was measured at 700 nm and the results were expressed as ascorbic acid equivalent.

2.6.4. Hydrogen peroxide activity H_2O_2

The hydrogen-donating activity, measured utilizing hydrogen peroxide radicals as the hydrogen acceptor was performed as previously described by Muruhan et al. [65] with minor modifications. Briefly a solution of hydrogen peroxide (40 mM) was prepared in phosphate buffer (pH 7.4). Different concentrations of the prepared compound (62.5, 31.25, 15.62, 7.81 and 3.9 μM) were added to a hydrogen peroxide solution (0.6 mL, 40 mM). The absorbance of hydrogen peroxide at 230 nm was determined after 10 min against a blank solution containing phosphate buffer without hydrogen peroxide (or ascorbic acid as the control). The hydrogen peroxide percentage activity was then calculated using the following equation:

$$H2O2\% = Ab' - \frac{Ab}{Ab'} \times 100$$

Where *Ab'* is the absorbance of the control reaction and *Ab* is the absorbance in the presence of the samples.

3. Results and discussions

The synthesis of the compound (NPOQA) is depicted in Scheme1. The starting material, 3-methylquinoxalin-2(1*H*)- one was prepared through treatment of *o*-phenylenediamine with sodium pyruvate in acetic acid [66]. This compound was proven to be a good synthons for different highly biologically active compounds. The lactam function of quinoxalinone is very reactive and so it condensed with 2–chloro-*N*-(4-methyl-2-nitrophenyl)acetamide. Structure of NPOQA was elucidated on the basis of spectral data.

Yield 80%, mp= 266.7 – 268.5 °C, **FT-IR** (ATR, υ, cm^{-1}): 3251 υ(N–H $_{amide}$), 1651 $\upsilon(C = O$ $_{amide})$, 833 υ(C–H_{arom}), 1601 $\upsilon(C{=}C_{arom})$, 1408 υ(C–H $_{CH3qin}$), 1470 $\upsilon(NO_2)$; **^{1}H NMR** (DMSO–d_6) δ ppm: 2.37 (3H, s, $CH_{3,quin}$); 2.49 (3H, s, $CH_{3,arom}$); 5.17 (2H, s, CH_2); 10.64 (1H, s, NH); 7.35–7.92 (m, J = 7.5 Hz, $7H_{Ar}$); **^{13}C NMR** (DMSO–d_6) δ ppm: 44.91 (CH_2–N_{Quin}); 19.99 ($CH_{3,arom}$); 21.11 ($CH_{3,Quin}$); 142.35 (C–NO_2); 165.45 ($C{=}O_{acetamid}$); 154.29 ($C = N_{,Quin}$); 157.57 ($C = O$ $_{quin}$). Its mass spectrum showed a molecular ion peak (MH^+, m/z = 353,12) which conforms to its molecular formula $C_{18}H_{16}N_4O_4$. SM (ESI+), IR and NMR spectra are given in the Supplementary Material Tables S1-S3.

The melting point was highly increased, compared to the precursor [66], yet our compound shown a moderate melting point if it was compared by the compounds of the same family [67–69]

On the basis of ^{1}H NMR spectrum which exhibited three signals at δ 2.49, 5.17 and 10.64 ppm referring to methyl group, CH_2 bound to the quinoxaline nitrogen and NH of acetamide group respectively, and revealed the absence of signal at δ 10.66 ppm corresponding hydrogen of the lactam which confirms the reaction between 3-methylquinoxalin-2(1H)-one and 2–chloro-N-(4-methyl-2-nitrophenyl) acetamide [69]. Its ^{13}C NMR spectrum showed signals at δ 19.99, 21.11, 44.91, 142.35,154.29, 157.57 and 165.45 referring to CH_3 of the phenyl ring, methyl group, CH_2 bound to quinoxaline nitrogen group, carbon liked to nitro group, $C = N$ of quinoxaline group, $C = O$ of quinoxaline group and Carbon of acetamide group respectively. IR spectrum of *NPOQA* showed band at 3251cm^{-1} for NH group and 1470 cm^{-1} due to NO_2 group, in addition the spectrum displayed absorption band at 1651 cm^{-1} characteristics for the carbonyle group. The elemental analyses and spectral data were in agreement with its structure.

3.1. X-ray crystallography

The quinoxaline moiety is slightly non-planar as seen by the dihedral angle of 1.4 (1)° between the mean planes of the constituent rings. The dihedral angle between the mean planes of the C1/C6/N1/C7/C8/N2 and the C12···C17 rings is 78.51(5)° while the nitro group is twisted from co-planarity with the latter ring by 16.5(1)°. The intramolecular N3—H3A···O3 hydrogen bond (Table 2 and Fig. 2) partially aids in determining the conformation of that portion of the molecule. The bond lengths and interbond angles are normal for the given formulation. In the crystal, thick chains of molecules extending along the *a*-axis direction are formed by N3—H3A···O2, C16—H16···O2 and C18—H18···O1 hydrogen bonds

Table 2
Hydrogen-bond geometry (Å, °).

Cg2 is the centroid of the C1···C6 benzene ring.

D—H···*A*	*D*—H	H···*A*	*D*···*A*	*D*—H···*A*
N3—H3A···O2^{i}	0.91	2.15	2.840(2)	132
N3—H3A···O3	0.91	2.03	2.647(2)	124
C10—H10B···Cg2^{i}	0.99	2.90	3.809(3)	153
C16—H16···O2ii	0.95	2.56	3.288(3)	134
C18—H18B···O1^{iii}	0.98	2.53	3.391(3)	146

Symmetry codes: (i) $x-1, y, z$; (ii) $-x+2, -y+1, -z$; (iii) $-x+1, -y+1, -z$.

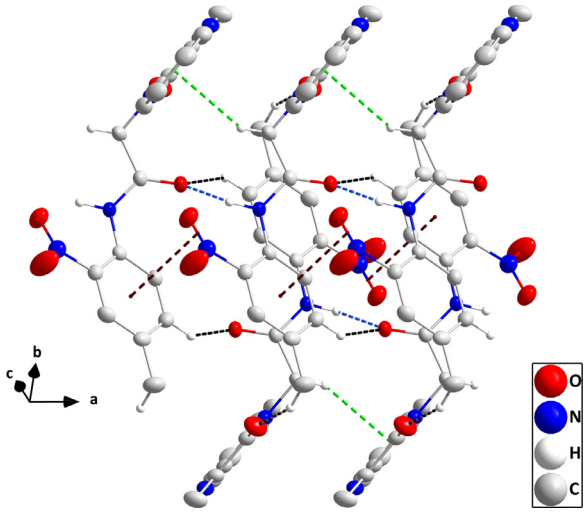

Fig. 2. Detail of the intermolecular interactions in a portion of one chain. N—H···O and C—H···O hydrogen bonds are depicted, respectively, by blue and black dashed lines while C—H···π(ring) and CO···π-ring interactions are shown, respectively, by green and purple dashed lines. (For interpretation of the references to colour in this figure legend, the reader is referred to the web version of this article.)

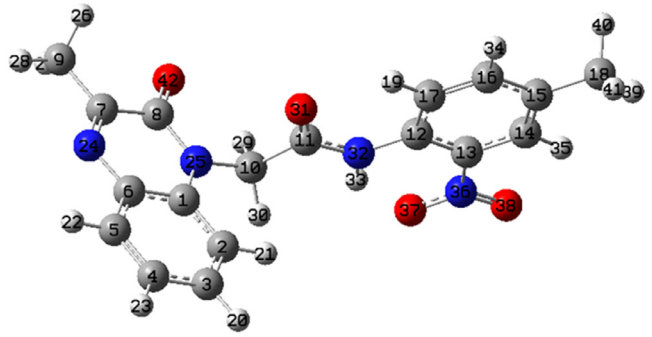

Fig. 3. The optimized structures of the compound NPOQA at B3LYP/6–311G** level.

together with C10—H10B···*Cg*2 interactions (Table 2 and Fig. 2) and assisted by π-stacking interactions between the N4O4 portion of the nitro group and the C12···C17 ring at $x-1, y, z$ (N4···ring centroid = 3.462(2) Å, O4···ring centroid = 3.330 (2) Å, N4O4···centroid = 85.85 (10)°).

3.2. Theoretical studies

3.2.1. Quantum chemical studies

The optimized and verified structure of the compound by the absence of the negative value in frequencies was presented in Fig. 3, and the physical quantities were summarized in Table 3. The dipole moment and polarizability behavior of the compound were affected by the solvent media, namely, they were estimated in 3.901 D and 253.048 au in the gas phase and in 5.291 D and 341.275 au in the water phase, due to the existence of the nitro (-NO_2) and carbonyl groups. Besides, the changing of the free energy of the compound implied that the compound had higher stability in the water (−1215.450046 au) phase than the gas (−1215.467289 au). The ΔE and ΔH quantities of the compound were computed as −1215.394590 au and −1215.371074 au in the gas and as −1215.411957 au and −1215.388460 au in the water. $\Delta E_{thermal}$ (in kcal/mol), Cv (in cal/molK), and S (in cal/molK) values were calculated as 215.818, 85.677, and 166.210 in the gas, whereas they were predicted as 215.593, 85.729, and 165.910, respectively.

Table 3
The calculated physiochemical quantities of the compound at B3LYP/6–311G** level.

	Gas	Water
DM (debye)	3.901	5.291
α (au)	253.048	341.275
ΔE (au)	−1215.394590	−1215.411957
ΔH (au)	−1215.371074	−1215.388460
ΔG (au)	−1215.450046	−1215.467289
$\Delta E_{thermal}$ (kcal/mol)	215.818	215.593
Cv (cal/molK)	85.677	85.729
S (cal/molK)	166.210	165.910

3.2.2. Natural bond orbital study

NBO analysis provides highly descriptive information about the reactivity behavior of organic [70–72] and inorganic systems [73–75] by predicting possible intermolecular interactions. Table 4 summarized the interactions that had the higher energy contributions to the lowering of the stabilization energy. Accordingly, the charge flow to aromatic ring from each of the lone pairs of the nitrogen atoms were determined as the highest contributions to $E^{(2)}$, which were LP (1) N25 (ED_i = 1.59816e) → Π* C1-C6 (ED_j = 0.44453e) and LP (1) N32 (ED_i = 1.64156e) → Π* C12-C13 (ED_j = 0.46356e) with the energies of 38.35 and 43.35 kcal/mol, respectively. Besides, the Π C12-C13 → Π* N36-O38 (ED_j = 0.61901e) interaction was determined by the energy of 30.95 kcal/mol, remarkable. Also, the charge flow to each of antibonding orbitals Π* C14-C15 (ED_j = 0.29765e) and Π* C16-C17 (ED_j = 0.27819e) from filled orbital Π C12-C13 had a striking energy of 20.07 and 14.00 kcal/mol, respectively. The $E^{(2)}$ values for the charge movement to each of Π* C2-C3, Π* C4-C5, and Π* C7-N24 unfilled orbitals from Π C1-C6 filled orbital were calculated as 17.03, 18.97, 12.61 kcal/mol, respectively. The $E^{(2)}$ values for the other resonance interactions occurred in the nitro substituted aromatic rings were calculated as 19.00, 20.85, 23.93, and 17.67 kcal/mol for the interactions of Π C14-C15 → Π* C12-C13, Π C14-C15 → Π* C16-C17, Π C16-C17 → Π* C12-C13, and Π C16-C17 → Π* C12-C13, respectively. Also, the $E^{(2)}$ values for Π C7-N24→ Π* C1-C6 and Π C7-N24→ Π* C8-O42 interactions were predicted as 14.77 and 13.34 kcal/mol, respectively.

3.2.3. Global reactivity study

Global reactivity identifiers obtained from the (*I*) and (*A*) values have been widely applied to a lot of scientific disciplines to evaluate the chemical behavior of the organic [76–79] and/or inorganic [80–82] molecular systems. In this study, the calculated reactivity parameters were given in Table 5. Accordingly, HOMO energy of the compound decreased whereas the LUMO energy increased, in the water simulation media. Thus, the energy gap of the compound was enlarged in the water phase in comparison to the gas phase. The E_{HOMO} and E_{LUMO} energies of the compound were calculated as −6.391 and −2.995 eV in gas and as −6.508 and −2.975 eV in the water, respectively. It can be said that the compound is more reactive in the water phase because of the larger ΔE value, that is, the ΔE values of the compound are calculated

Table 4
NBO analysis results of the compound at B3LYP/6–311G** level.

Donor(i) Gas	ED_i/e	Acceptor (j)	ED_j/e	$E^{(2)}$/ kcalmol^{-1}	E(j)-E(i)/ a.u	F(i,j)/ a.u
Π C1-C6	1.57496	Π* C2-C3Π* C4-C5Π* C7-N24	0.329290.298680.18842	17.0318.9712.61	0.290.300.29	0.0640.0690.057
Π C2-C3	1.70495	Π* C1-C6Π* C4-C5	0.444530.29868	21.2316.62	0.280.30	0.0720.063
Π C4-C5	1.68763	Π* C1-C6Π* C2-C3	0.444530.32929	18.2022.49	0.270.28	0.0650.071
Π C7-N24	1.84750	Π* C1-C6Π* C8-O42	0.444530.33158	14.7713.34	0.340.33	0.0690.062
Π C12-C13	1.63515	Π* C14-C15Π* C16-C17Π* N36-O38	0.297650.278190.61901	20.0714.0030.95	0.310.310.15	0.0720.0600.064
Π C14-C15	1.66361	Π* C12-C13Π* C16-C17	0.463560.27819	19.0020.85	0.260.29	0.0650.070
Π C16-C17	1.67441	Π* C12-C13Π* C14-C15	0.463560.29765	23.9317.67	0.260.29	0.0730.065
LP (1) N25	1.59816	Π* C1-C6	0.44453	38.35	0.29	0.095
LP (1) N32	1.64156	Π* C12-C13	0.46356	43.35	0.27	0.099

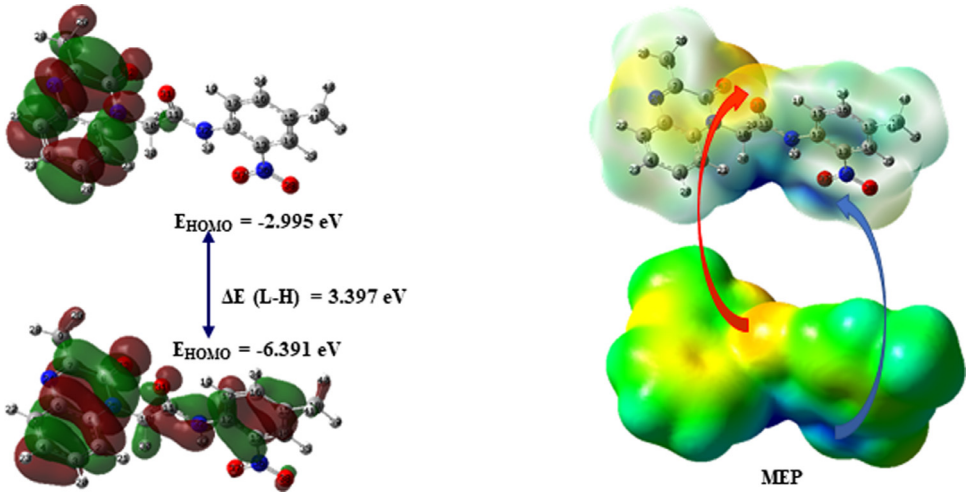

Fig. 4. HOMO& LUMO (isoval:0.02), and MEP (isoval:0.0004) pilots of the compound at B3LYP/6–311G** level in the gas phase.

Table 5
The quantum chemical parameters of the compound *NPOQA* at B3LYP/6–311G** level.

	Gas	Water
H (-I) (eV)	−6.391	−6.508
L (-A) (eV)	−2.995	−2.975
ΔE (L-H) (eV)	3.397	3.533
μ (eV)	−4.693	−4.741
η (eV)	1.698	1.766
ω (eV)	6.485	6.364
ΔN_{max} (eV)	2.763	2.684
$\Delta\varepsilon_{back\text{-}donat.}$ (eV)	−0.425	−0.442
ω^+ (au)	0.160	0.155
ω^- (au)	0.332	0.329

as 3.397 eV in gas and 3.533 eV in the water, respectively. Besides, the compound is harder in the water (1.766 eV) than the gas phase (1.698 eV). From Table 5, (ω) and ΔN_{max} indexes (in eV) were calculated higher in the gas (ω=6.485 and ΔN_{max}= 2.763) than the gas water (ω=6.364 and ΔN_{max}= 2.684). Also, the (ω^+) and (ω^-) indexes implied that the compound more likely prefer the electrodonating tendency than the electroaccepting behavior, in both phases. The (ω^+) and (ω^-) values of the compound were estimated as 0.160 and 0.332 in the gas and as 0.155 and 0.329 in the water media.

The HOMO, LUMO and MEP profiles of the compound were illustrated in Fig. 4 to give a clear picture for the nucleophilic (HOMO) and electrophilic (LUMO) attack sites. Except for the methyl groups and for oxygen atoms of the nitro group, HOMO density of the compound spread out overall molecular surface. On the other hand, LUMO density did lay out completely on the 3-methyl-2-oxoquinoxalin ring of the compound. Besides, MEP plots indicated that the electron-rich region (orange color) in moderate size covered the oxygen atoms, whereas the electron-poor region (blue color) of the compound coated the around of hydrogen atom of the secondary amin group. The remaining parts of the compound seem neutral for both the electrophilic and nucleophilic attack because of the green color, but there were sprinkle the slight positive potential (light blue) on the electron density surface of the compound *NPOQA*.

3.3. Enzyme inhibitory activities

In an array to explore the *in vitro* antidiabetic activity, quinoxaline derivative was screened for the α-amylase and α-glucosidase inhibitory properties. Effects were compared with the commercially available inhibitor, acarbose (Ac). Inhibitory activities of the compound were evaluated at different concentrations and results were given in Fig. 5A,B. Acarbose and *NPOQA* showed a dose dependent inhibitory effect on enzymes.

The results showed that the compound *NPOQA* had a remarkable inhibitory effect on α-glucosidase activity (**IC_{50} 83.78 ± 0.888 μM**). *NPOQA* has a dose-dependent inhibitory effect on α-glucosidase and it showed a statistically highly significant as $P < 0.001$, which is comparable to others *N*-aryl acetamides hybrid system [10,11], similar result was found for α-amylase. NPOQA showed a considerable activity (**IC_{50} 199.7 ± 0.952 μM**). Therefore, it considered as an active compound for this application (Table 6).

3.4. Antioxidant activity

In vitro antioxidant activity of NPOQA complexe was evaluated by using radical methods, DPPH, ABTS, FRAP, The antioxi-

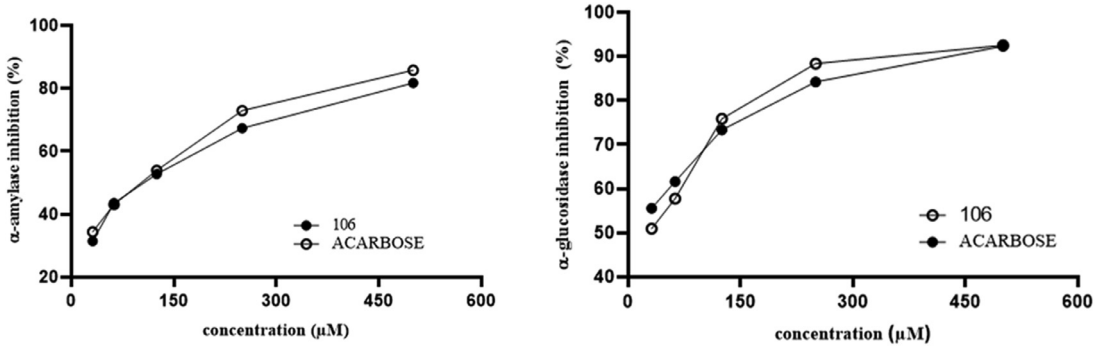

Fig. 5. **A**)α-amylase inhibitory activities of NPOQA**; B**) α-glucosidase inhibitory activities of NPOQA.

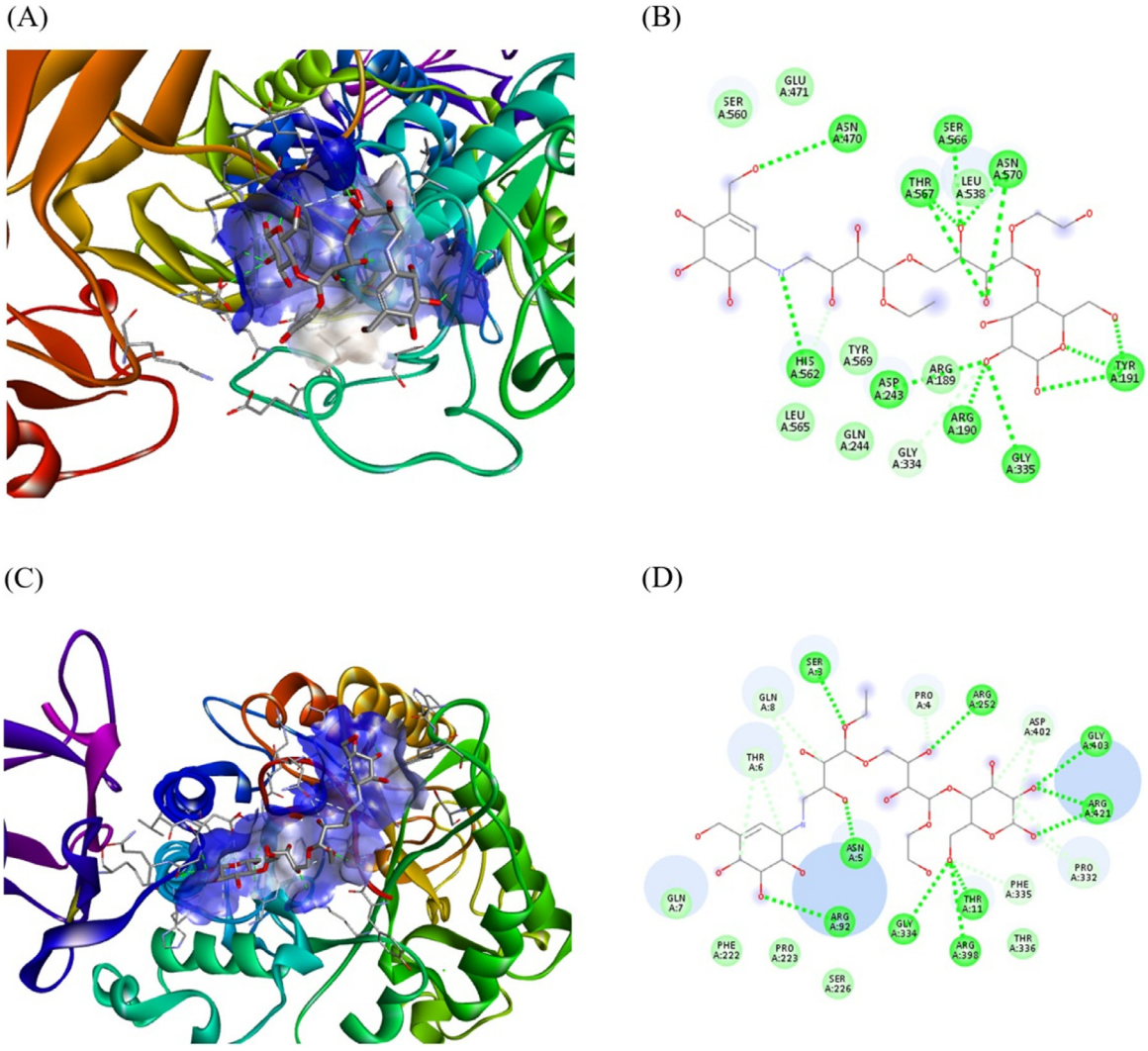

Fig. 6. Molecular docking of acarbose with α–amylase and α-glucosidase. (**A**) Binding of acarbose with glucosidase, (**B**) amino acid residues and various interactions involved in acarbose-glucosidase complex, (**C**) binding of acarbose with -amylase (**D**) amino acid residues and various interactions involved in acarbose-amylase complex.

Table 6
IC_{50} of the *NPOQA* enzyme inhibitory activity:.

	(IC_{50} µmol/ml)	
Compound	α-glucosidase	α-amylase
NPOQA	83.78 ± 0.888****	199.7 ± 0.952****
Acarbose	72.58 ± 0.682	115.6 ± 0.574

Values represent mean ± standard deviation ($n = 3$).
Values with the same superscript on the same row are significantly similar (P (<0,0001)).

dant property of the tested samples was evaluated at different concentrations and Ascorbic Acid was used as a standard for the comparison of the activity. The obtained result of DPPH assay showed a good antioxidant activity, with IC50 value (104, 1 ± 4, 65 μM), while IC50 value of ascorbic acid (78, 11±0, 68 μM). The NPOQA have developed an important antioxidant activity in the ABTS test, and better than other similar heterocyclic compounds [13]. With a correlation to the antioxidant activity shown in the DPPH test (Table 7), it showed the average antioxidant ability

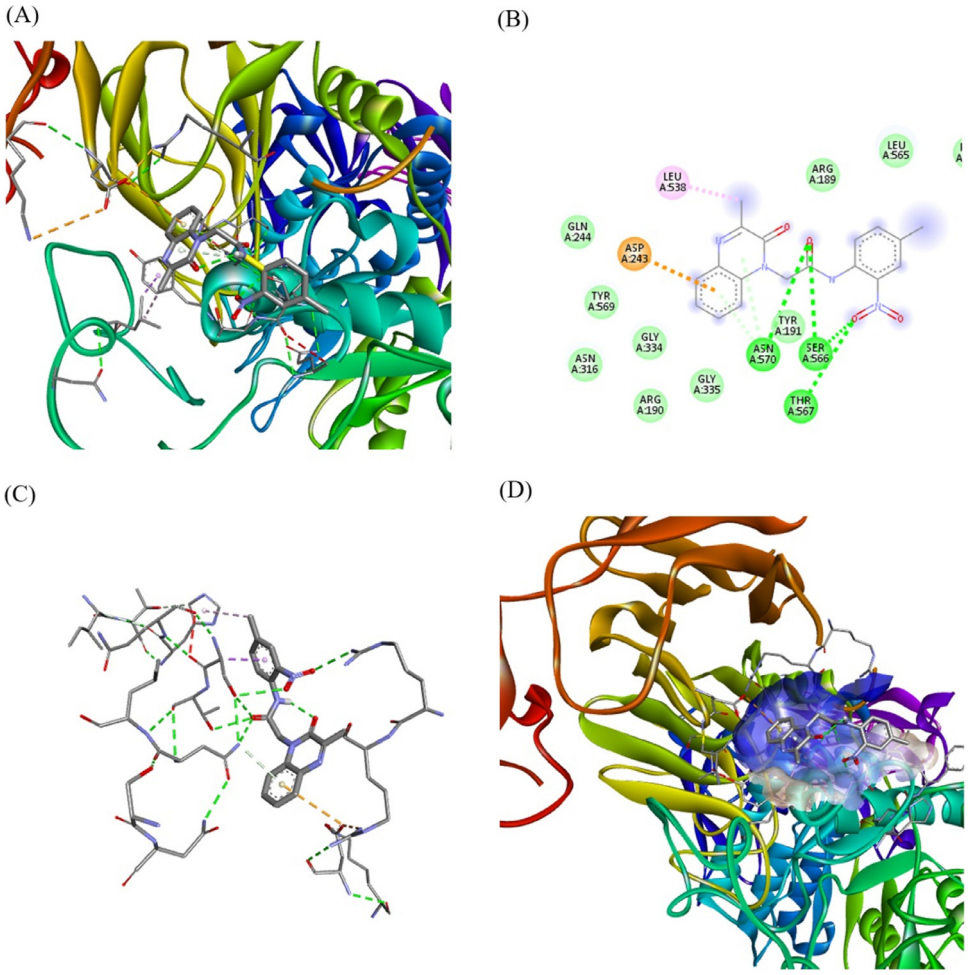

Fig. 7. Molecular docking of *NPOQA* with α-glucosidase. (**A**) Binding of *NPOQA* with α-glucosidase, (**B**) (2D) amino acid residues and various interactions involved in *NPOQA*-glucosidase complex, (**C**) (3D) amino acid residues and various interactions involved in *NPOQA*-glucosidase complex, (**D**)binding of *NPOQA* with glucosidase hydrophobic pocket.

Table 7
Antioxidant activities (DPPH, ABTS, FRAP and H_2O_2) of *NPOQA*. Data are expressed as mean ± SD ($n = 3$).

	DPPH (IC_{50} µM)	ABTS (µM AAE)	FRAP (µM AAE)	H_2O_2 (IC_{50} µM)
NPOQA	104,1 ± 4,65	330,30 ± 3,44	298,54±6,59	5,06±0,48
Ascorbic Acid	78,11±0,68	-	-	7,45±1,11

(330,30 ± 3,44 µM AA). Moreover, in the FRAP method, the highest reducing power was interestingly observed also in the NPOQA (298,54±6,59 µM AAE). The FRAP value indicates that the compound has a ferric reducing antioxidant power and it has a relatively high antioxidant activity compared to compounds of the same family [8]. The synthesized compound NPOQA demonstrated a strong activity, with IC50 value (5,06±0,48 μM), while IC50 value of ascorbic acid (7,45±1,11 μM).

3.5. Molecular docking

Molecular docking study was performed to analyze the binding modes of the studied compound against α-glucosidase and α-amylase enzyme. The results showed that both acarbose and *NPOQA* were able to bind to the active site of α-glucosidase, the calculated binding energy was found to be −6.5 and −6.9 kcal/mol successively for acarbose and *NPOQA* (Table 8). Several hydrogen bonded interactions were observed between various hydroxyl groups of acarbose and amino acids Ser3, Pro312, Arg252, Gly403,

Table 8
.The calculated binding energy for acarbose and *NPOQA*.

Acarbose glucosidase	Glucosidase Affinity kcal/mol	Risidus	Amylase Affinity kcal/mol	Risidus
acarbose	−6.5	ASN470, THR567, SER566, LEU538, ASN570, TYR191, GLY335, ARG190, ARG189, ASP243, HIS562	−6.6	THR6,GLN8, SER3,PRO4, ARG252,ASP402,GLY403,ARG421, PRP332, PHE335, THR336, THR11, ARG398, GLY334, ASN5, ARG92
NPOQA	−6.9	Leu538, asp243, ASN570, TYR191, SER566, THR56	−7.6	ASP402,ARG398, SER289, TYR333, ARG421, PRO332

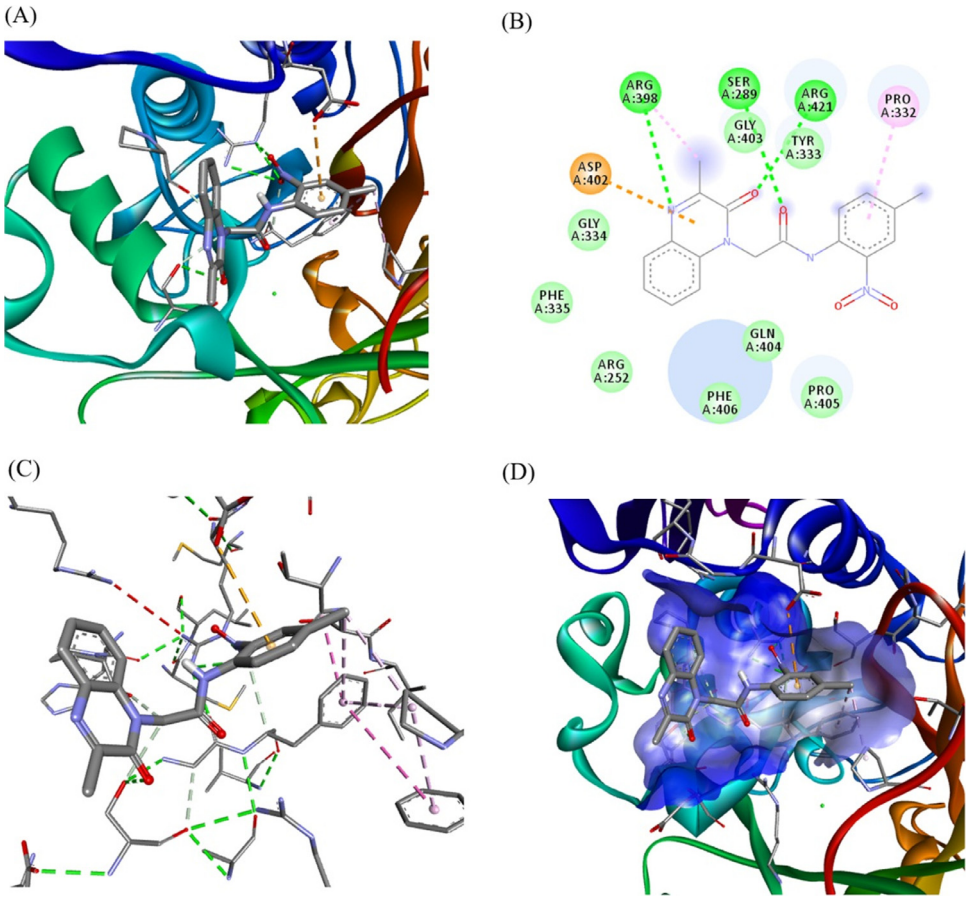

Fig. 8. Molecular docking of NPOQA with Amylase. (**A**) Binding of *NPOQA* with amylase, (**B**) (2D) amino acid residues and various interactions involved in NPOQA-amylase complex, (**C**) (3D) amino acid residues and various interactions involved in acarbose-amylase complex, (**D**)binding of *NPOQA* with amylase hydrophobic pocket.

Arg421, Thr 11, Arg398, Gly334, Asn5 and Arg5 of α-glucosidase enzyme (Fig. 6). Exploration of molecular interaction of *NPOQA* shows several hydrogen's bonds (Asn570, Tyr191, Ser566, Thr567), Pi-anion interactions with Asp243, and a Pi-alkyl interaction between the methyl and Leu538. The studied compound *NPOQA* was well accommodated in the binding pocket of α-glucosidase as shown in Fig. 7. Results showed that compound *NPOQA* has an important binding affinity as compared to standard drug acarbose. Which are in agreement with the results of *in vitro* studies.

We have also performed molecular docking of *NPOQA* and acarbose with α–amylase. The calculated binding affinity was predicted to be −6.6 and −7.6 Kcal/mol successively for acarbose and *NPOQA* (Table 8)**.** Compound *NPOQA* was lockted at the hydrophobic pocket of the enzyme (Fig. 8). Surrounded by the residues ASP-402, ARG-398, SER-289, TYR-333, ARG-421, PRO-332 forming a stable hydrophobic binding. Detailed analysis showed that the methyl group in position 3 of the *NPOQA* formed π-alkyl interactions with the residues Arg-398 in addition to an π-anion and π-alkyl between phenyl group and residues Asp-402 and Pro-332. All these interactions helped *NPOQA* to anchor in the binding site of the α-amylase and explain the higher binding affinity compared to acarbose. The magnitude of the binding affinity and the different interactions indicates that the studied compounds *NPOQA* and acarbose interacted strongly with α -amylase, confirming the *in vitro* data.

4. Conclusion

In this research, new quinoxaline derivative, *N*-(4-methyl-2-nitrophenyl)−2-(3-methyl-2-oxoquinoxalin-1(2H)-yl)acetamide (NPOQA) has been synthesized, with significant yield and characterized by different spectroscopic techniques. The structure was resolved by the XRD analysis and this illustrates that the quinoxaline unit is not quite planar. FMO analyses revealed that the electrodonating potency (0.332au) of the compound was greater than the electroaccepting capability (0.160au) in both phases. In addition, the HOMO density of the compound expanded on the whole molecular surface more than the LUMO, and the 3-methyl-2-oxoquinoxalin ring was liable for the electrophilic attacks. NBO analyses showed that the n→ Π* and Π→ Π* interactions were greatly responsible for the decreasing of the stabilization energy. The compound NPOQA was evaluated for its *in vitro* antidiabetic and antioxidant activities ; It showed an excellent antidiabetic and antioxidant activities. In addition to this, molecular docking studies were carried to investigate the binding mode between NPOQA and the two enzymes, α-glucosidase and α-amylase. Thus, this study explores, theoretical prediction, antidiabetic, antioxidant activities and docking studies of quinoxaline-*N*-aryl acetamide hybrid system for development of potential multifunctional medicinal candidates.

Author contributions

Mohcine Missioui: Performed experiments, Wrote a draft the paper. (Chemical section).

Salma Mortada: Performed experiments, Wrote a draft the paper. (Biological section).

Walid Guerrab: Performed the molecular docking study

Goncagül Serdaroğlu: Performed the X-ray crystallographic analysis, wrote the paper.

Savaş Kaya: Performed the computational chemistry analysis.

Joel T. Mague: Collected and processed the X-ray data
El Mokhtar Essassi: Conceptualization, methodology.
M. E. Abbes Faouzi: Supervision (Biological section).
Youssef Ramli: Conceptualization, methodology, supervision, Wrote the paper.

Declaration of competing interest

The authors of this manuscript have no conflict of interest to declare.

Acknowledgments

Authors are grateful to Mohammed V University and to Scientific and Technological Research Council of Turkey (TUBITAK). All quantum chemical calculations were performed at High Performance and Grid Computing Center (TR-Grid e-Infrastructure). The support of NSF-MRI Grant #1228232 for the purchase of the diffractometer and Tulane University for support of the Tulane Crystallography Laboratory are gratefully acknowledged.

Supplementary materials

Supplementary material associated with this article can be found, in the online version, at doi:10.1016/j.molstruc.2021.130484.

References

[1] C.T. Walsh, Nature loves nitrogen heterocycles, Tetrahedron Lett 56 (2015) 3075e3081, doi:10.1016/j.tetlet.2014.11.046.
[2] H. Kuo, W. Ko, Y. Hsu, G. Lee, C.K. Lai, Mesogenic heterocycles derived from quinoxaline Schiff Bases, Tetrahedron 72 (2016) 6321e6333, doi:10.1016/j.tet.2016.07.076.
[3] H. Kuo, Y. Chen, G. Lee, C.K. Lai, Symmetric quinoxaline e oxadiazole conjugates: mesogenic behavior via quinoxaline -CH interactions, Tetrahedron 72 (2016) 6843e6853, doi:10.1016/j.tet.2016.09.011.
[4] K. Lin, H. Kuo, H. Sheu, C.K. Lai, Unsymmetric 1,3,4-oxa(thia)diazoles of quinoxalineenaphthalene conjugates, Tetrahedron 69 (2013) 9045e9055, doi:10.1016/j.tet.2013.08.031.
[5] E.J. Foster, R.B. Jones, C. Lavigueur, V.E. Williams, Structural factors controlling the self-assembly of columnar liquid crystals, J. Am. Chem. Soc. 128 (2006) 8569e8574, doi:10.1021/ja0613198.
[6] Y. Ramli, E.M. Essassi, Advances in synthetic approaches, functionnalization and biological properties of quinoxaline derivatives, in: Advances in Chemistry Research Ed, 27, James C. Taylor Nova Science Publishers, New York., 2015, pp. 109–160.
[7] Y. Ramli, A. Moussaif, K. Karrouchi, E.M. Essassi, Pharmacological profile of quinoxalinone, J. Chem. (2014) 1–21 2014 Article ID 563406, doi:10.1155/2014/563406.
[8] U.P. Tarpada, B.B. Thummar, D.K. Raval, A green protocol for the synthesis of quinoxaline derivatives catalyzed by polymer supported sulphanilic acid, Arabian Journal of Chemistry 10 (2017) 2902 -290, doi:10.1016/j.arabjc.2013.11.021.
[9] K. Saravana Mani, B. Murugesapandian, W. Kaminsky, S.P. Rajendran, Enantioselective approach towards the synthesis of spiro-indeno [1,2-b] quinoxaline pyrrolothiazoles as antioxidant and antiproliferative, Tetrahedron Lett. 59 (2018) 2921–2929, doi:10.1016/j.tetlet.2018.06.035.
[10] G. Wang, X. Li, J. Wang, Z. Xie, L. Li, M. Chen, S. Chen, Y. Peng, Synthesis, molecular docking and a-glucosidase inhibition of 2-((5,6-diphenyl-1,2,4-triazin-3-yl) thio)-N-arylacetamides, Bioorg. Med. Chem. Lett. 27 (2017) 1115–1118, doi:10.1016/j.bmcl.2017.01.094.
[11] S. Moghimi, M. Toolabi, S. Salarinejad, L. Firoozpour, S. Esmaeil, S. Ebrahimi, F. Safari, S. Mojtabavi, M.A. Faramarzi, A. Forouma, Bioorg. Chem. 102 (2020) 104071, doi:10.1016/j.bioorg.2020.104071.
[12] R.M. Asath, T.N. Rekha, S. Premkumar, T. Mathavan, A. Milton, Franklin Beni, J Mol Struct 1125 (2016) 633–642, doi:10.1016/j.molstruc.2016.07.064.
[13] L. Wolf, N. Quoos, J.C.P. Mayer, D. de Souza, A.C. Sauer, V.Bortolotto L.Meichtry, M. Prigol, O.E.D. Rodrigues, L. Dornelles, Synthesis and free radical scavenging activity of 2-alkyl/arylchalcogenyl-N-(4-aryl-1,3-thiazol-2-yl)acetamide compounds, Tetrahedron Lett. 57 (2016) 1031–1034, doi:10.1016/j.tetlet.2016.01.079.
[14] S. Koppireddi, J.R. Komsani, S. Avula, S. Pombala, S. Vasamsetti, S. Kotamraju, R. Yadla, Novel 2-(2,4-dioxo-1,3-thiazolidin-5-yl)acetamides as antioxidant and/or anti-inflammatory compounds, Eur J Med Chem 66 (2013) 305–313, doi:10.1016/j.ejmech.2013.06.005.
[15] M. Nazir, M.A. Abbasi, S.Z.Siddiqui Aziz-ur-Rehman, K.M. Khan, U. Salar, M. Shahid, M. Ashraf, M.A. Lodhi, F.A. Khan, Bioorg. Chem. 81 (2018) 253–263, doi:10.1016/j.bioorg.2018.08.010.
[16] International Diabetes Federation. IDF Diabetes Atlas, 9th edn., Brussels, Belgium: International Diabetes Federation, 2019 Available at https://idf.org/aboutdiabetes/what-is-diabetes/facts-figures.html Acess 20/07/2020.
[17] M. Brownlee, The pathobiology of diabetic complications, Diabetes 54 (2005) 1615–1625, doi:10.2337/diabetes.54.6.1615.
[18] L. Cansigno, E.E. Hernández-Domíngueza, J.L. Monribot-Villanueva, A.F. Licea–Navarro, L.E. Mateo-Cid, A. Segura-Cabrera, J.A. Guerrero-Analco, Screening of Mexican tropical seaweeds as sources of α-amylase and α-glucosidase inhibitors Cristina, Algal Res 49 (2020) 101954.
[19] M.A.H. Salahuddina, A. Ismaila, N. KKassim, M. Hamid, M.S.M. Ali, Food Chem 331 (2020) 127240, doi:10.1016/j.foodchem.2020.127240.
[20] N. Jaradat, S.Abdallah N.Al-Maharik, R. Shawahna, A. Mousa, A. Qtishat, Ind Crops Prod 158 (2020) 112946, doi:10.1016/j.indcrop.2020.112946.
[21] E. d. Santos Pereira, J.R. Vinholes, T.M. Camargoa, F.R. Nora, R. Lopes, C.F. Chaves, L.N.M. Vizzotto, Food Biosci 37 (2020) 100665, doi:10.1016/j.fbio.2020.100665.
[22] X. Liu, Y. Wang, J. Zhang, L. Yan, S. Liu, A. A.Taha, J. Wang, M. Chao, J Supercrit Fluids 158 (2020) 104747, doi:10.1016/j.supflu.2019.104747.
[23] X. Gu, Y. Yang, Z. Wang, South African Journal of Botany 133 (2020) 151–160, doi:10.1016/j.sajb.2020.07.021.
[24] M. Alomari, M. Taha, M.Selvaraj F.Rahim, N. Iqbal, S. Chigurupati, S. Hussain, N. Uddin, N.B. Almandil, M. Nawaz, R.K. Farooq, K.M. Khan, Synthesis of indole-based-thiadiazole derivatives as a potent inhibitor of α-glucosidase enzyme along with in silico study, Bioorg. Chem. 108 (2021) 104638, doi:10.1016/j.bioorg.2021.104638.
[25] S. Hussain, M. Taha, F. Rahim, S. Hayat, K. Zaman, N. Iqbal, M. Selvaraj, M. Sajid, M.A. Bangesh, F. Khan, K.M. Khan, N. Uddin, S.A.A. Shah, M. Ali, J Mol Struct (2021), doi:10.1016/j.molstruc.2021.130029.
[26] Z. Tavaf, S.K. Dangolanib, R. Yousefi, F. Panahib, M.B. Shahsavani, A. Khalafi-Nezhad, Carbohydr. Res. 494 (2020) 108069, doi:10.1016/j.carres.2020.108069.
[27] Y. Zaoui, Y. Ramli, E.R.T.Tiekink S.L.Tan, L. Chemlal, J.T. Mague, J. Taoufik, M.E.A. Faouzi, M.H. Ansar, Synthesis, structural characterisation and theoretical studies of a novel pyridazine derivative: investigations of anti-inflammatory activity and inhibition of α-glucosidase, J Mol Struct 1234 (2021) 130177, doi:10.1016/j.molstruc.2021.130177.
[28] N. Abad, H.H. Sallam, F.H. Al-Ostoot, H.A. Khamees, S.A. Al-horaibi, S.A. Khanum, M. Madegowda, M. El Hafi, J.T. Mague, E.M. Essassi, Y. Ramli, Synthesis, crystal structure, DFT calculations, Hirshfeld surface analysis, energy frameworks, molecular dynamics and docking studies of novel isoxazolequinoxaline derivative (IZQ) as anti-cancer drug, J Mol Struct 1232 (2021) 130004, doi:10.1016/j.molstruc.2021.130004.
[29] N. Abad, S. Ferfra, E.M. Essassi, J.T. Mague, Y. Ramli, Synthesis and crystal structure of 1-octyl-3-phenylquinoxalin-2 (1H)-one, C22H26N2O, Zeitschrift für Kristallographie-New Crystal Structures 236 (2021) 173–175, doi:10.1515/ncrs-2020-0404.
[30] W. Guerrab, M. Missioui, Y. Zaoui, J.T. Mague, Y. Ramli, Synthesis and crystal structure of 2-azido-N-phenylacetamide, C8H8N4O, Zeitschrift für Kristallographie-New Crystal Structures 236 (2021) 133–134, doi:10.1515/ncrs-2020-0409.
[31] W. Guerrab, H. Lgaz, S. Kansiz, J.T. Mague, N. Dege, M. Ansar, R. Marzouki, I.H.Ali J.Taoufik, I.M. Chung, Y. Ramli, Synthesis of a novel phenytoin derivative: crystal structure, Hirshfeld surface analysis and DFT calculations, J Mol Struct 1205 (2019) 127630, doi:10.1016/j.molstruc.2019.127630.
[32] Bruker *APEX3SAINT, SADABS* & *SHELXTL*, Bruker AXS, Inc., Madison, WI, 2016.
[33] G.M. Sheldrick, Acta Cryst A71 (2015) 3–8, doi:10.1107/S2053273314026370.
[34] G.M. Sheldrick, Acta Cryst C71 (2015) 3–8, doi:10.1107/S2053229614024218.
[35] K. Brandenburg, H. Putz, DIAMOND, Crystal Impact GbR, Bonn, Germany, 2012.
[36] G.M. Sheldrick, TWINABS, University of Göttingen, Göttingen, Germany, 2009.
[37] A.D. Becke, Density-functional thermochemistry. III. The role of exact exchange, J. Chem. Phys. 98 (1993) 5648–5652, doi:10.1063/1.464913.
[38] C. Lee, W. Yang, R.G. Parr, Development of the Colle-Salvetti correlation-energy formula into a functional of the electron density, Phys. Rev. B 37 (1988) 785–789, doi:10.1103/physrevb.37.785.
[39] K. Raghavachari, J.S. Binkley, R. Seeger, J.A. Pople, Self-Consistent Molecular Orbital Methods. 20. Basis set for correlated wave-functions, J. Chem. Phys. 72 (1980) 650–654, doi:10.1063/1.438955.
[40] A.D. McLean, G.S. Chandler, Contracted Gaussian-basis sets for molecular calculations. 1. 2nd row atoms, Z=11-18, J. Chem. Phys. 72 (1980) 5639–5648 https://doi.org/10.1063/1.438980.
[41] B. Mennucci, J. Tomasi, Continuum solvation models: a new approach to the problem of solute's charge distribution and cavity boundaries, J. Chem. Phys 106 (1997) 5151–5158.
[42] J. Tomasi, B. Mennucci, R. Cammi, Quantum mechanical continuum solvation models, Chem. Rev. 105 (2005) 2999–3093, doi:10.1021/cr9904009.
[43] E. Cancès, B. Mennucci, J. Tomasi, A new integral equation formalism for the polarizable continuum model: theoretical background and applications to isotropic and anistropic dielectrics, J.Chem. Phys 107 (1997) 3032–3041, doi:10.1063/1.474659.
[44] T. Koopmans, Über die Zuordnung von Wellenfunktionen und Eigenwerten zu den Einzelnen Elektronen Eines Atoms, Physica. 1 (1934) 104–113, doi:10.1016/S0031-8914(34)90011-2.
[45] R.G. Parr, L.V. Szentpaly, S. Liu, Electrophilicity Index, J. Am. Chem. Soc. 121 (1999) 1922–1924.
[46] R.G. Parr, R.G. Pearson, Absolute hardness: companion parameter to absolute electronegativity, J. Am. Chem. Soc. 105 (1983) 7512–7516, doi:10.1021/ja00364a005.

[47] R.G. Pearson, Absolute electronegativity and hardness correlated with molecular orbital theory, Proc. Natl. Acad. Sci. USA 83(1986) 8440–8441. https://doi.org/10.1073/pnas.83.22.8440
[48] I. Nazmul, S. Kaya (Eds.), Conceptual Density Functional Theory and Its Application in the Chemical Domain, CRC Press, 2018.
[49] J.L. Gazquez, A. Cedillo, A. Vela, Electrodonating and Electroaccepting Powers, J. Phys. Chem. A100 (2007) 1966–1970, doi:10.1021/la8033676.
[50] B. Gomez, N.V. Likhanova, M.A. Domínguez-Aguilar, R. Martínez-Palou, A. Vela, J.L. Gazquez, Quantum Chemical Study of the Inhibitive Properties of 2-Pyridyl-Azoles, J. Phys. Chem. B110 (2006) 8928–8934, doi:10.1021/jp057143y.
[51] A.E. Reed, L.A. Curtiss, F. Weinhold, Intermolecular interactions from a natural bond orbital, donor-acceptor viewpoint, Chem. Rev. 88 (1988) 899–926, doi:10.1021/cr00088a005.
[52] A.E. Reed, F. Weinhold, Natural Localized Molecular Orbitals, J. Chem. Phys. 83 (1985) 1736–1740, doi:10.1063/1.449360.
[53] A.E. Reed, R.B. Weinstock, F. Weinhold, Natural-population analysis, J. Chem. Phys. 83 (1985) 735–746, doi:10.1063/1.449486.
[54] J.P. Foster, F. Weinhold, Natural hybrid orbitals, J. Am. Chem. Soc. 102 (1980) 7211–7218, doi:10.1021/ja00544a007.
[55] M.J. Frisch, G.W. Trucks, H.B. Schlegel, G.E. Scuseria, M.A. Robb, J.R. Cheeseman, G. Scalmani, V. Barone, B. Mennucci, G.A. Petersson, H. Nakatsuji, M. Caricato, X. Li, H.P. Hratchian, A.F. Izmaylov, J. Bloino, G. Zheng, J.L. Sonnenberg, M. Hada, M. Ehara, K. Toyota, R. Fukuda, J. Hasegawa, M. Ishida, T. Nakajima, Y. Honda, O. Kitao, H. Nakai, T. Vreven, J.A. Montgomery Jr., J.E. Peralta, F. Ogliaro, M. Bearpark, J.J. Heyd, E. Brothers, K.N. Kudin, V.N. Staroverov, T. Keith, R. Kobayashi, J. Normand, K. Raghavachari, A. Rendell, J.C. Burant, S.S. Iyengar, J. Tomasi, M. Cossi, N. Rega, J.M. Millam, M. Klene, J.E. Knox, J.B. Cross, V. Bakken, C. Adamo, J. Jaramillo, R. Gomperts, R.E. Stratmann, O. Yazyev, A.J. Austin, R. Cammi, C. Pomelli, J.W. Ochterski, R.L. Martin, K. Morokuma, V.G. Zakrzewski, G.A. Voth, P. Salvador, J.J. Dannenberg, S. Dapprich, A.D. Daniels, O. Farkas, J.B. Foresman, J.V. Ortiz, J. Cioslowski, D.J. Fox, Gaussian 09 W, Revision D.01, Gaussian, Inc, Wallingford CT, 2013.
[56] GaussView 6.0.16, Gaussian Inc., Wallingford CT, 2016.
[57] A. Hashim, M.S. Khan, M.S. Khan, M.H. Baig, S. Ahmad, Antioxidant and α-Amylase inhibitory property of phyllanthus virgatus L.: an *in vitro* and molecular interaction study, Biomed Res. Int. 2013 (2013) 12, doi:10.1155/2013/729393.
[58] K.T. Kee, M. Koh, L.X. Oong, K. Ng, Screening culinary herbs for antioxidant and alphaglucosidase inhibitory activities, Int. J. Food Sci. Technol. 48 (2013) 1884–1891, doi:10.1111/ijfs.12166.
[59] O. Trott, A.J. Olson, AutoDock Vina: improving the speed and accuracy of docking with a new scoring function, efficient optimization, and multithreading, J Comput Chem 31 (2010) 455–461 Available at, doi:10.1002/jcc.21334.
[60] L.K. Williams, Order and disorder: differential structural impacts of myricetin and ethyl caffeate on human amylase, an antidiabetic target, Journal of medicinal chemistry. ACS Publications 55 (2012) 10177–10186, doi:10.1021/jm301273u.
[61] V. Roig-Zamboni, Structure of human lysosomal acid α-glucosidase–a guide for the treatment of Pompe disease, Nature communications. Nature Publishing Group 8 (2017) 1–10.
[62] B. Huang, H. Ke, J. He, X. Ban, H. Zeng, Y. Wang, Extracts of Halenia elliptica exhibit antioxidant properties *in vitro* and *in vivo*, Food and Chemical Toxicology 49 (2011) 185–190, doi:10.1016/j.fct.2010.10.015.
[63] C.I.G. Tuberoso, M. Boban, E. Bifulco, D. Budimir, F.M. Pirisi, Antioxidant capacity and vasodilatory properties of Mediterranean food: the case of Cannonau wine, myrtle berries liqueur and strawberry-tree honey, Food Chem 140 (2013) 686–691, doi:10.1016/j.foodchem.2012.09.071.
[64] R. Amarowicz, R.B. Pegg, P. Rahimi-Moghaddam, B. Barl, J.A. Weil, Free-radical scavenging capacity and antioxidant activity of selected plant species from the Canadian prairies, Food Chem 84 (2004) 551–562, doi:10.1016/S0308-8146(03)00278-4.
[65] S. Muruhan, S. Selvaraj, P.K. Viswanathan, *In vitro* antioxidant activities of Solanum surattense leaf extract, Asian Pac J Trop Biomed 3 (2013) 28–34, doi:10.1016/S2221-1691(13)60019-2.
[66] I.V. Nikolaenko, O.Q. Munro, 3-Methyl-1*H*-quinoxalin-2-one, Acta Cryst E60 (2004) 92–94, doi:10.1107/S1600536803028368.
[67] Y.S. Xu, C.C. Zeng, X.M. Li, R.G. Zhong, 3-{ [4-(4 Methylphenylsulfonamido)benzoyl]methylidene}-3,4-dihydroquinoxalin-2(1H)-one, Acta Cryst E61 (2005) 3802–3804, doi:10.1107/S1600536805033301.
[68] M.A.Z. El-Attar, R.Y. Elbayaa, O.G. Shaaban, N.S. Habib, A.E. Abdel Wahab, I.A. Abdelwahab, S.A.M. El-Hawash, Design, synthesis, antibacterial evaluation and molecular docking studies of some new quinoxaline derivatives targeting dihyropteroate synthase enzyme, Bioorg. Chem. 76 (2018) 437–448, doi:10.1016/j.bioorg.2017.12.017.
[69] H.A.S. Abbas, A.R. Al-Marhabi, S.I. Eissa, Y.A. Ammar, Molecular modeling studies and synthesis of novel quinoxaline derivatives with potential anticancer activity as inhibitors of c-Met kinase, Bioorg. Med. Chem. 23 (2015) 6560–6572, doi:10.1016/j.bmc.2015.09.023.
[70] M. Elik, G. Serdaroğlu, A Computational Study of 1-Substituted Methyl 9-Methyl-9H-Pyrido [3,4-b]indole-3-Carboxylate: quantum Chemical Descriptors, FMO and NBO, Cumhuriyet Science Journal 38 (2017) 138–155, doi:10.17776/csj.356185.
[71] L. Bejaoui, A. Brahmia, R. Marzouki, M. Dusek, V. Eigner, G. Serdaroğlu, S. Kaya, M. El Bour, R. Ben Hassen, Synthesis, crystal structure, hirshfeld surface analysis, spectroscopic, biological and first-principles studies of novel aminocoumarins, J Mol Struct 1221 (2020) 128862, doi:10.1016/j.molstruc.2020.128862.
[72] G. Serdaroğlu, N. Uludağ, The electronic and spectroscopic investigation of (±)-Dasycarpidone, Vib Spectrosc 111 (2020) 103156, doi:10.1016/j.vibspec.2020.103156.
[73] N. Şahin, G. Serdaroğlu, S.D. Düşünceli, M.N. Tahir, C. Arıcı, İ. Özdemir, Direct arylation of eteroarenes by PEPPSI-type palladium–NHC complexes and representative quantum chemical calculations for the ompound which the structure was determined by X-ray crystallography, J. Coord. Chem. 72 (2019) 3258–3284, doi:10.1080/00958972.2019.1692202.
[74] J.M. Jacob, M.R.P. Kurup, K. Nisha, G. Serdaroğlu, S. Kaya, Mixed ligand copper(II) chelates derived from an O, N, S- donor tridentate thiosemicarbazone: synthesis, spectral aspects, FMO, and NBO analysis, Polyhedron 189 (2020) 114736, doi:10.1016/j.poly.2020.114736.
[75] N.A. Mangalama, M.R.P. Kurup, E. Suresh, S. Kaya, G. Serdaroğlu, Diversities in the chelation of aroylhydrazones towards cobalt(II) salts: synthesis, spectral characterization, crystal structure and some theoretical studies, J. Mol. Struct. (2021) 129978 (in press), doi:10.1016/j.molstruc.2021.129978.
[76] G. Serdaroğlu, S. Kaya, R. Touir, Eco-friendly sodium gluconate and trisodium citrate inhibitors for low carbon steel in simulated cooling water system: theoretical study and molecular dynamic simulations, J. Mol. Liq. 319 (2020) 114108, doi:10.1016/j.molliq.2020.114108.
[77] M. Bouklah, H. Elmsellem, Krim, G. Serdaroğlu, B. Hammouti, A. Elidrissi, S. Kaya, I. Warad, Effect of substitution on corrosion inhibition properties of three Imidazole derivatives on mild steel in 1 M HCl, Arab. J. Chem. Environ. Res. 07 (2017) 126–143.
[78] L. Guo, X. Ren, Y. Zhou, S. Xu, Y Gong, S. Zhang, Theoretical evaluation of the corrosion inhibitionperformance of 1,3-thiazole and its aminoderivatives, Arab. J. Chem. 10 (2017) 121–130, doi:10.1016/j.arabjc.2015.01.005.
[79] G. Serdaroğlu, M. Elik, DFT Based Quantum Chemical Descriptors of 1-Substituted THβC, DHβC, βC Derivatives, Cumhuriyet Sci. J 38 (2017) 647–660, doi:10.17776/csj.349241.
[80] A. Üngördü, N. Tezer, Electronic Properties of Artificial Metal-DNA Base Pair Complexes Formed from Hydroxypyridone Base, Chemistry Select 5 (2020) 7267–7276, doi:10.1002/slct.201904232.
[81] K. Sayın, M. Rezaeivala, Modelling studies on the investigation of non-linear optical properties of some Ex^{n}Box cyclophanes, Cumhuriyet Sci. J. 41 (2020) 344–350, doi:10.17776/csj.683463.
[82] E. Üstün, S.D. Düşünceli, İ. Özdemir, Theoretical analysis of frontier orbitals, electronic transitions, and global reactivity descriptors of M $(CO)_4$ L_2 type metal carbonyl complexes: a DFT/TDDFT study, Struct. Chem. 30 (2019) 769–775, doi:10.1007/s11224-018-1231-0.